RESEARCH ARTICLE

In vivo x-ray diffraction and simultaneous EMG reveal the time course of myofilament lattice dilation and filament stretch

Malingen SA[1], Asencio AM[1], Cass JA[2], Ma W[3], Irving TC[3] and Daniel TL[1]

ABSTRACT

Muscle's function within an organism depends on molecular to meter scale actions that feed back upon one-another. While the motions of the contractile machinery are well described in isolated muscle preparations, only a handful of experiments have documented the kinematics of the lattice occurring when multi-scale interactions are fully intact. We used time-resolved x-ray diffraction to record the kinematics of the myofilament lattice within a normal operating context: the tethered flight of *Manduca sexta*. Since the primary flight muscles of *Manduca sexta* are synchronous, we used these results to reveal the timing of *in vivo* cross bridge recruitment, which occurred 19 ms (SD: 11) ms following activation. In addition, the thick filaments stretched an average of 0.4% (SD: 0.2%) and thin filaments stretched 0.5% (SD: 0.4%). In contrast to other *in vivo* preparations, lattice spacing changed an average of 1.5% (SD: 0.7%). The scale of these kinematics indicates that they are important for *in vivo* force generation. While kinematics were consistent within individual trials, there was extensive variation between trials that might be explained by a host of latent variables occurring in naturally functioning systems. The diverse kinematic combinations we documented mirror muscle's adaptability, and may facilitate its robust function in the face of unpredictable operating conditions.

KEYWORDS: sarcomere, structure-function, myofilament lattice dynamics

Using the same foundational molecular machinery, muscle performs diverse functions within an organism; at turns functioning as a motor, structural support, a repository for elastic energy, or as a shock absorber (1). A muscle's functional output – the force it creates and its length change – depends upon multi-scale interactions. Arrays of molecular motors interact (generating piconewton scale forces) in a feedback loop with interacting muscle groups (generating newton scale forces) within the animal's body. The highly organized lattice of contractile machinery which powers contraction also changes shape as a result of internal forces, temperature, and externally applied forces. In turn, the shape of the lattice tunes force production. For instance, increasing the spacing between molecular motors and the thin filaments to which they bind decreases binding probability, and therefore decreases force output (2). The spacing of the lattice co-varies with naturally occurring temperature gradients, and has the potential to shift the function of otherwise identical muscle sub-units from motors to springs and dampers (3; 4). The thick and thin filaments which house myosin molecular motors and their actin binding sites have also been shown to be far from a rigid system; instead, they stretch as as a result of internal axial forces. Though the measured extensions are small, they have non-trivial mechanical implications, accounting for about 70% of muscle's total compliance (5), and resulting in increased binding probability due to changes in the axial register of molecular motors and prospective binding sites (6). While lattice dilation and filament stretch are known to have profound mechanical implications (7), the relationship of their magnitude and timing within a naturally functioning organism has remained enigmatic. To address this, we documented molecular motor recruitment following nervous activation, and the resulting filament stretching and changes in lattice spacing in a novel *in vivo* experimental system: the synchronous flight muscles of the hawkmoth *Manduca sexta*.

The advent of high-speed digital detectors in the early 2000's made *in vivo*, time resolved x-ray diffraction possible. Landmark studies of lattice kinematics in naturally functioning systems have largely focused on asynchronous insect flight muscles (fruitfly: *Drosophila* and bumblebee: *Bombus*) (8; 9; 10). Irving & Maughan (9), for example, were the first to document the molecular kinematics of a mutant fly *in vivo*, connecting molecular mutations with their functional outcomes across the scales of animal flight behavior. However one limitation of these systems is that in asynchronous muscle neural activation is decoupled from cycles of muscle shortening and lengthening; instead, activation serves to keep the muscle in a contractile state by continuously suffusing myofibrils with calcium ions. Asynchronous muscle is uniquely

[1]University of Washington: Biology
[2]Allen Institute for Cell Science
[3]Illinois Institute of Technology

Authors for correspondence: sage701@uw.edu

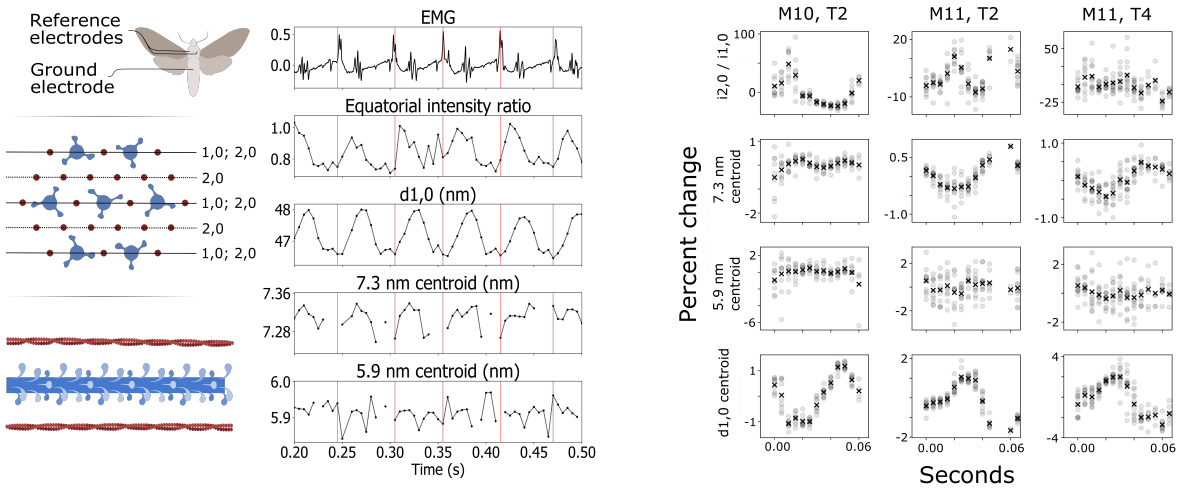

(a) Simultaneous EMG and x-ray diffraction traces.

(b) STAs vary between individuals.

Fig. 1. (a) The muscle's activation recorded in the EMG signal is indicated by a vertical red line. Cross bridge recruitment was inferred by the radial shift of mass between the 1,0 and 2,0 planes as cross bridges move towards the thin filaments following activation. Lattice spacing was measured using the 1,0 reflection. Thick filament stretching was inferred from changes in the spacing of the 7.3 nm meridional reflection and thin filament stretching from changes in the axial spacing of the 5.9 nm off-meridional reflection. (b) Data was phase averaged using the muscle's endogenous depolarization. The mean of each time point following activation is marked with an X.

specialized to power high-frequency wing flapping (11). Iwamoto and Yagi leveraged this to record the mechanism of stretch activation independent of calcium release and re-uptake (10). In contrast to asynchronous muscle, many mammalian skeletal muscles are activated in partial tetany, with multiple neural impulses stimulating larger contractile forces. Vertebrate cardiac muscle, on the other hand, has a one-to-one relationship between activation and contraction. In a manner analogous to cardiac muscle, the dominant flight muscles of *Manduca sexta* are synchronous with, generally, a one-to-one correspondence between neural activation and muscle contraction. Additionally, they mirror cardiac muscle in their function, contracting against fluid loads and acting predominantly on the ascending portion of their length-tension curve (12).

By pairing simultaneous recording of muscle activation with x-ray diffraction data, we were able to phase average lattice kinematics using the organism's natural activation. These results uniquely show the timing of molecular motor recruitment and the resulting lattice kinematics (stretching and dilation) following activation. Using phase averaged data we found that the molecular kinematics are consistent within individuals, often showing large excursions: the lattice can dilate by as much as 1.26 nm (2.7%), thick filaments can stretch by as much as 0.8%, and thin filaments by as much as 1.2%. The magnitude of these results support the idea that lattice kinematics significantly modulate muscle function. As is expected in a fully intact, normally functioning animal, there was considerable variation in both the timing and extent of lattice motions across individuals. These results highlight that while individuals may manifest the same functional outcome at the organism scale (flight), the mechanics of the lattice underneath can vary. In light of this, lattice kinematic data need to be considered within the context of individuals without supposing that latent variables are equal across individuals (13).

RESULTS AND DISCUSSION

We recorded cross bridge recruitment, axial filament strains and radial lattice dilation as a function of endogenous muscle activation during *in vivo* tethered flight. These were indicated respectively by: the ratio of the intensities of the 2,0 to the 1,0 equatorial reflections; axial shifts of the centroid of the 7.3 nm meridional reflection and axial shifts of the 5.9 nm actin off meridional reflection and finally radial shifts in the position of the equatorial reflections (Fig: 3). With a detector frame rate of 200 Hz and wing beat frequencies ranging between 10-18 Hz (mean 15 (SD: 2) Hz), we obtained 11-20 x-ray diffraction images from each cycle of shortening and lengthening. Each trial lasted one second, and a Spike Triggered Average (STA) was created by phase averaging the data based on the peaks of each individual's Electromyogram (EMG). Most individuals had consistent STAs, however there was variability between individuals in the time course and excursions of their STAs for a given data type (Figs: 1, S1). The excursion of a signal was calculated as the difference between the maximum and minimum of the STA for each trial.

Cross bridge recruitment

While the timing of the excitation contraction pathway has been recorded in isolated fibers (14), the time course of cross bridge recruitment following activation *in vivo* has not previously been reported. Muscle contraction is triggered by motor neuron activation, leading to depolarization of the muscle cell membrane and the subsequent release of calcium from the sarcoplasmic reticulum into the cytoplasm surrounding the filament lattice. Calcium binding initiates the shifting of the troponin - tropomyosin complex away from actin binding sites and the dissociation of molecular motors from the thick filament, allowing the formation of cross bridges between the filaments (15; 16; 17). Our data show that peak cross bridge recruitment occurs an average of 0.019 (SD: 0.011) seconds following activation, to a resolution of 0.005 seconds. While the time course of cross bridge recruitment was generally consistent in an individual trial over many cycles of sequential shortening and lengthening, there was variation between individuals, resulting in the large standard deviation.

The variation in lattice kinematics that we recorded in a fully intact system could arise from several latent variables. For example, temperature varies both spatially and temporally in *Manduca sexta*. Temperature gradients correlate with variation in lattice kinematics at the molecular scale, and molecular scale variation corresponds to functional gradients across the muscle group at the organism scale (3). In addition to gradients across a muscle group, the mean temperature of the muscle group increases with increasing wing beat frequency in *Manduca sexta* (18). Temperature may contribute to the observed variation in our system since the diffusion of substrates like calcium ions and molecular motors is slower in cool muscle. However the experimental constraints of simultaneous EMG recordings and high speed, time-resolved x-ray diffraction in a naturally functioning animal limit our ability to resolve spatio-temporal patterns of temperature in the muscle. In favor of an intact preparation, we did not control temperature and all of the moths were flapping their wings at different frequencies of their own volition. While temperature is a likely contributes to the variation we observe in our data, diversity in the timing of maximum cross bridge recruitment could also arise from other mechanisms, such as other steps in the excitation-contraction pathway, or co-occurring lattice spacing changes and filament stretching.

Although the ratio of the intensities of the 2,0 and 1,0 reflections is often used to quantify the shifting of mass between them (19), peak intensities could in theory be affected by changes in lattice ordering (20) over a cycle of shortening and lengthening. Additionally, shifting of mass from the thick to the thin filaments does not necessarily imply binding. However, despite these caveats, the shifting of mass is well correlated with strong motor binding in vertebrate muscle (7; 21). Since *Manduca sexta*'s myofilament lattice is so well ordered, this ratio is an accessible surrogate for cross bridge recruitment during time resolved x-ray diffraction.

Filament stretching

Filament stretching, which arises from internal axial forces, profoundly impacts muscle's function. Axial filament stretching accounts for a large component of the sarcomere's total compliance (about 70% (5)), enabling the return of stored elastic strain energy. The stretching of filaments also means that cross bridges do not act independently of one another. Instead, as the relative space between binding sites and cross bridges changes, binding probability is also altered. Spatially explicit modeling demonstrates that these changes in axial register may mediate force output (6).

However the extent of filament stretch occurring during natural muscle function was unknown until recent evidence from time-resolved x-ray diffraction revealed subtle (0.2 %) thick filament stretching in the dominant flight muscles of *Drosophila* (8). Our measurements show that the thick filament stretches by an average 0.4% (SD: 0.2%) across 10 trials as indicated by changes in the 7.3 nm meridional intensity peak (Fig: 3). While the symmetry of *Manduca sexta*'s thick filament is not yet known it may be different from vertebrate filaments, akin to *Lethocerus*, which has a four stranded thick filament (22; 23). Thus the 7.3 nm reflection should not be assumed to be exactly equivalent to the M6 reflection in vertebrate muscle. In analogy with vertebrate muscle, the 7.3 nm reflection likely includes contributions from the second order of

Summary of data				
Data type	Number of trials	Excursion (nm)	Excursion (proportion of mean)	Peak time (s)
Equatorial intensity ratio	9	0.139 (SD: 0.142)	0.160 (SD: 0.136)	0.019 (SD: 0.011)
Thick filament backbone spacing	7	0.028 (SD: 0.016)	0.004 (SD: 0.002)	0.057 (SD: 0.023)
Thin filament pitch spacing	6	0.032 (SD: 0.024)	0.005 (SD: 0.004)	0.046 (SD: 0.026)
Lattice spacing	10	0.708 (SD: 0.307)	0.015 (SD: 0.007)	0.028 (SD: 0.009)
Cross bridge crown spacing	6	0.160 (SD: 0.096)	0.011 (SD: 0.007)	0.039 (SD: 0.026)

Table 1. For each of the 11 total trials, and each data type we ran a permutation test to see if there was a significant frequency component at wing beat frequency. If the chance of a random permutation yielding a power as high or higher than the raw data at wing beat frequency was less than 5% we factored it into this summary. If it was greater than 5% we can only conclude that if there are periodic changes occurring, they are of lower amplitude than the noise envelope.

the 14.4 nm myosin head repeat with additional contributions from the thick filament backbone. The imperfect correlation of the 7.3 nm reflection and the 14.4 nm reflection indicates that the spacing change of the 7.3 nm is dominated by structures in the backbone, and can therefore be used as a measure of thick filament extensibility (Fig: S2; Supplement: The 7.3 nm repeat as a metric of thick filament backbone spacing). Though larger than those observed in *Drosophila*, these values are well within the range of extensions observed in isolated vertebrate fibers under isometric contraction (5; 24; 25). This confirms the relevance of these parameters to *in vivo* function in a synchronous muscle group during natural function. Additionally, by measuring the extension of filaments within individuals rather than averaging across trials, the blunting of the signal that occurs when averaging phase offset data is avoided.

Lattice dilation

Muscle function is also impacted by the spacing of the myofilament lattice, which is thought to play a role in the Frank-Starling mechanism in the mammalian heart (26). Cross bridge binding alters lattice spacing, and in turn their binding probability and the direction of the forces they generate is regulated by lattice spacing (27). Radial cross bridge extension has also been proposed as a site of elastic energy storage that could be returned to power cyclic contraction (28; 3). Through mechanisms such as these, lattice spacing change results in a steeper length tension curve than would be produced if only filament overlap changed during contraction (29). Since these muscles act on the steep ascending portion of their length tension curve they generate larger forces in response to perturbations that stretch them, without a need to modify nervous control. Therefore when blood pressure suddenly rises and increases ventricular filling, or a gust of wind buffets against a wing, the muscle autonomously responds by generating a larger contractile force. This is an example of a cell-scale set point that yields a reflexive response to environmental perturbations at the organism scale, lending robust response to rapidly changing external demands (26).

Isolated muscle preparations have yielded mixed interpretations of how lattice spacing changes over the course of a contraction, although it is clear that lattice spacing is influenced by both mechanical and electrostatic interactions (30). Often the lattice is assumed to have either a constant spacing during contraction, or to be isovolumetric. But these assumptions don't capture the extent of lattice spacing change observed experimentally. For instance, in skinned fiber preparations it was shown that during force generation lattice spacing tended toward a spacing near that observed when the membrane was intact (31). Meanwhile it was shown in relaxed, intact vertebrate muscle fibers that the sarcomere can be approximated as being isovolumetric, but when cross bridges are active both axial tension and sarcomere length are determinants of lattice spacing (32). Are lattice spacing changes occurring during *in vivo* muscle function?

The average lattice spacing excursion we measured across 11 trials was 1.5% (SD: 0.7%), corresponding to 0.708 nm (SD: 0.307 nm). These data stand in contrast to the results of Irving *et al* (9), which showed no measurable lattice spacing change in the flight muscles of *Drosophila* to a resolution of 0.05 nm; the equivalent of $\pm 0.1\%$ lattice spacing change in their system. While these are significant changes in spacing, they are much smaller than the approximately 4% change in spacing needed to maintain a constant volume based upon the strains of this muscle group measured by Tu *et al* (about 9% (12)). The average lattice spacing change we measured corresponds to an alteration in the force generated in osmotically compressed demembranated myofibrils of approximately 8% (2). We therefore expect that lattice spacing change can be an important determinant of the force produced by this muscle group. Moreover, the maximum lattice spacing excursion we recorded was nearly twice the mean (1.26 nm). Akin to cross bridge recruitment and filament stretching, lattice spacing change followed a stereotyped time course within individual trials, but the time course of lattice dilation demonstrated great breadth across trials. Similar parameters to those noted for cross bridge recruitment and filament stretch may also give rise to the variation we observed in lattice spacing.

Interrelationship of lattice kinematics

Our kinematic data capture filament motions within a mechanically coupled system. Since filament strain is caused by cross bridge binding, we hypothesized that the stretching of the thick filament indicated by movement of the 7.3 nm meridional reflection would correlate with increased cross bridge binding. Surprisingly, the correlation between cross bridge recruitment and thick filament stretch shows variable timing offsets across individual trials, demonstrating a more complicated relationship between these variables. This may be partially explained by recent work which demonstrates that there is a non-linear relationship between tension and thick filament extension (33). Proteins similar to titin may also contribute to sarcomere elasticity in *Manduca sexta* (34) with significant non-linear behavior (35; 36; 37) and temperature dependence (38). Finally, while stretching of the filaments indicates internal axial force, cross bridges also exert force radially. This means that the magnitude of the component of cross bridge force applied axially changes as function of the angle between motors and binding sites (27; 29). In light of these considerations, it would be remarkable if the movement of mass towards the thin filaments alone explained the periodic stretching of the thick filaments, or the periodic dilation of the lattice. But taken together, can we use these data to fully model the system?

If the data are sufficient to explain one another mechanistically, even though the linkage is non-obvious, they should be sufficient to train a mechanism-free, data-based model. (Though by creating a mechanism free model we cannot exclude the possibility that the data are insufficient to explain one another mechanistically, but contain enough correlative information to successfully predict one-another.) We used a gradient boosting decision tree algorithm housed in the XGBoost library (39) to train a mechanism free model. First we trained the model with 75% of a trial's data, using the other 25% as a test set to evaluate model performance. We set up the model to predict lattice spacing from filament stretching and cross bridge recruitment since lattice spacing is typically the cleanest of the signals tracked in x-ray diffraction due to its intensity. In addition to using the current state of filament stretch and cross bridge recruitment to predict the current lattice spacing, we also provided the model with the time history of the predictor variables up to 6 time steps (.03 s) previous to the current state. For these within-trial predictions the random forest based model performed well, with an average explained variance above zero, demonstrating that it is possible to predict lattice spacing change from filament stretching and cross bridge recruitment within a trial.

We then addressed our larger question – can we create a prediction of lattice spacing change from cross bridge recruitment and filament stretching data that holds across individuals? We iteratively withheld the data from one individual as a test case and trained the model with the data from all other individuals. For each with-held trial the model failed to create a prediction with an explained variance ratio above zero. This shows that the themes the model uses to create intra-individual predictions do not generalize across individuals.

It is possible that cross bridge recruitment, filament strain and lattice dilation are sufficient to explain the system, but that the data we gathered don't capture a sufficient range of the possible kinematic combinations. However it seems likely that there are other components of the system needed to link lattice kinematics together. These components could be latent variables like

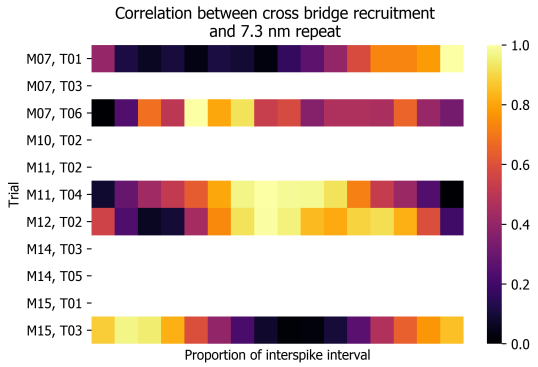

(a) Correlation of cross bridge recruitment and thick filament stretch

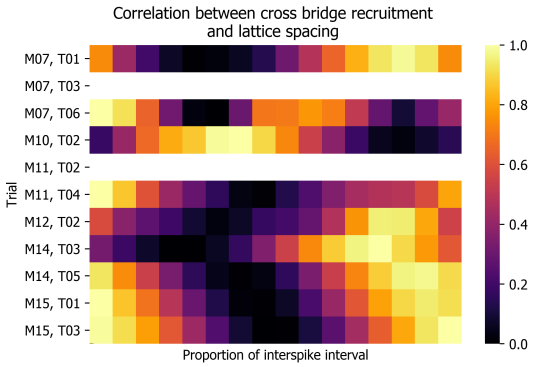

(b) Correlation of cross bridge recruitment and lattice dilation

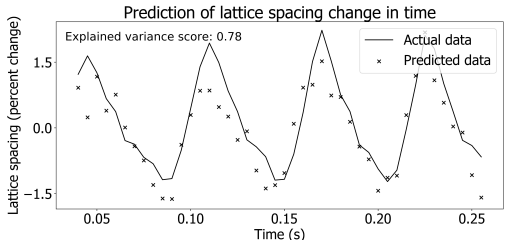

(c) A mechanism free model creates a good prediction of lattice spacing change on untrained lattice spacing data when it is trained and tested using data from the same trial, but different time points.

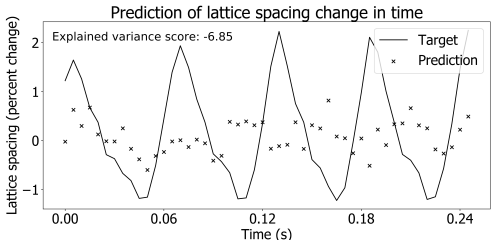

(d) The same mechanism free model framework fails to create an adequate prediction of lattice spacing change when the model is trained on all trials but one and tested on the with-held trial.

Fig. 2. Panel a) shows that there is not a consistent phase offset of cross bridge recruitment and filament stretch (indicated by the 7.3 nm repeat). The magnitude of the correlation is normalized, and phase offset is measured in proportion of the interspike interval. Some trials do not contain adequate data for all data pairings – a permutation bootstrap was used to determine for each datatype within a trial if it contained a significant periodic component at wingbeat frequency, and those that did were included. Correlation as a function of time lag in seconds can be found in the Supplement (Fig: S4). Panel b) shows the correlation between cross bridge recruitment and lattice spacing. Panels c) and d) show a mechanism free model's prediction of lattice spacing from filament strains and cross bridge recruitment in time. Panel c) shows a prediction for the case where the model is trained on 75% of a trial's data, and tested on the other 25%. The average explained variance across all trials was 0.25 (SD: 0.72) (the average root mean square error was 0.67 SD: 0.25) Panel d) shows a representative image from the case where the model was trained on the data from all trials, except for one that was with-held as a test set. The mean explained variance across all trials trained in this manner was -3.70 (SD: 2.76) (the average root mean square error was 1.03 SD: 0.30). The disparity between c) and d) demonstrates that while this model is capable of making good predictions from these types of data sets (panel c), the predictions made by the model cannot extrapolate across individuals.

temperature, externally applied forces, timing of activation, and antagonistic muscle activation. This demonstrates that the myofilament lattice uses a panoply of kinematic combinations, the breadth and significance of which we have yet to grapple with, during natural function.

CONCLUSION

At the organism scale, muscle is known to exhibit diverse functionality; at turns acting to power motion, to stabilize the body and to store or absorb energy (1). This diverse functionality is enabled by feedback between molecular and organism scale dynamics. We recorded the kinematics of the lattice during natural function at all scales, revealing that thick filaments stretch 0.4% (SD: 0.2%) and the lattice dilates 1.5% (SD: 0.7%). By using a novel preparation, the synchronous flight muscles of *Manduca sexta*, we were able to record that peak cross bridge recruitment occurs 19 ms (SD: 11 ms) after activation *in vivo*. Despite the uncertainties of inherent in interpreting x-ray diffraction data from a muscle group whose ultrastructure has yet to be resolved, this system holds great promise for understanding the *in vivo* operating paradigm in a muscle with function similar to human cardiac muscle, and resolving the timing of lattice kinematics with respect to activation. We recorded extensive variation between individuals in the timing and extent of lattice kinematics that could not be predicted by a powerful, mechanism free model. Variation could arise from features like temperature, the timing of muscle activation and the interaction of many muscles in the animal's body. While we cannot pinpoint the source of the variation we observed, it points to the need to explore how muscle uses a broad palette of kinematics to produce functional movement in a constantly changing environment.

MATERIALS AND METHODS

Animal preparation

To record cross bridge recruitment and lattice kinematics as a function of electrical activation we used an insect synchronous muscle. The dorsal longitudinal muscles (DLMs) of *Manduca sexta* are synchronously activated, and are an excellent system for x-ray diffraction experiments since the thorax is composed of about a cubic centimeter of highly ordered muscle, and the exoskeleton produces negligible scattering. The exceptionally clear diffraction patterns produced with this muscle made it possible to collect time resolved data without frame averaging. We used a random mix of male and female moths between 1-2 weeks post eclosion.

We cold anesthetized a moth, tethered it, and then placed it in the beam line (Figure 3). Each moth was unencumbered except by Electromyography (EMG) electrodes inserted into the thorax and a ventral tether. The tether was a flattened stainless steel needle coated in cyanoacrylate glue inserted between the second and third coxae and crystalized with sodium bicarbonate. The moth was positioned on the tether with a pitch angle of approximately 30° to the horizon, similar to natural flight orientation. The moth was placed on the beamline with its body axis, and hence the axis of the dorsal longitudinal muscles, at a right angle to the beam's incidence. The beam passed through the anterior, dorsal quadrant of the thorax, intersecting at approximately the d-c DLM subgroup based on external morphology (40). It was aimed consistently in a small section where the wings would not obstruct the beam path. A hot air soldering iron set to its lowest heat setting was placed approximately 1m in front of the moth while a fan with a filter attached was placed behind the moth to collect dislodged scales. The warmth of the soldering iron and the wind current created by it and the fan stimulated natural flight behavior and kept the moth warmer than the room's cool ambient temperature.

Electromyogram

EMG electrodes with hooked tips were inserted into the posterior of the thorax after puncturing the exoskeleton with a needle. The ground electrode was inserted into the abdomen 3.

X-ray diffraction

Beamline setup

The experiment was performed at the Biophysics Collaborative Access Team (BioCAT), beamline 18ID at the Advanced Photon Source, Argonne National Laboratory, Lemont, IL, USA (41). The beam energy was 12.0 keV with an incident flux of 10^{13} photons/s and attenuated as needed to 10^{12} photons/s. It was focused to 250x250 μm at the animal's thorax, and 60x150 μm at the detector with a sample to detector distance of 2 m. The sample

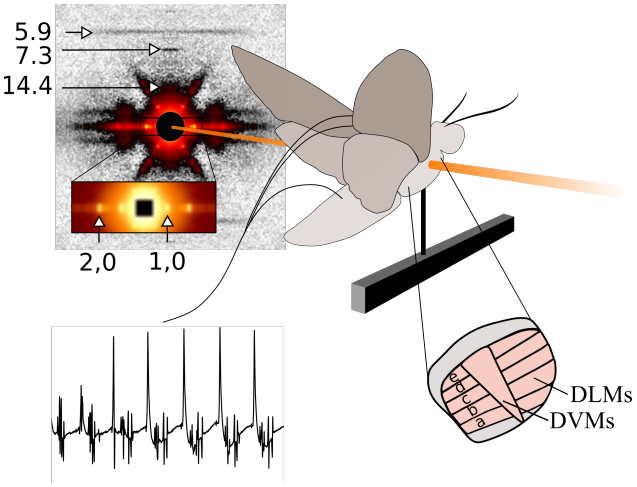

Fig. 3. The moth was tethered within the beamline such that the beam passed through the dorsal-anterior portion of the thorax where the DLM's comprise the bulk of the tissue volume. Simultaneous EMG data was collected to measure membrane depolarization. The x-ray diffraction image shown is after convex hull background subtraction, which leaves the reflections due to periodic structures intact, but removes the decaying intensity around the backstop due to the beam's dispersion.

was oscillated over a 1 mm excursion in the beam at $20 - 30$ mm/s in order to mitigate radiation damage. This method of oscillating the tissue relies upon the supposition that all sarcomeres in a local region are behaving in the same manner, so moving the sample will not alter the x-ray periodicities observed. We used a photon counting Pilatus 3 1M (Dectris Inc.) with 981x1043, 172x172 μm, pixels with a 20-bit dynamic range.

Raw image data was collected at 200 Hz with 1 ms of dead time per frame, and with the X-ray shutter open continuously.

Data reduction from x-ray diffraction images

The 32-bit tagged image file format (TIFF) image stacks returned by the x-ray detector were annotated using the Musclex software suite developed by the Biophysics Collaborative Access Team (BioCAT) (42). Images were annotated by two different individuals and cross-validated to ensure that there was not a substantial difference between them (Fig: S4). Each image was quadrant folded to center and average intensities across axes of symmetry and annotated for meridional and equatorial intensity peaks. We used versions of Musclex prior to version 1.14.12. An improvement in centering is being implemented in future versions which reduces the error inherent in interpreting physically continuous data recorded in a pixel framework (Supplement: Sources of error and cross validation).

Cross bridge recruitment

Cross bridge recruitment can be inferred by the shifting of mass away from the thick filaments and towards the thin filaments. Since the flight muscle of *Manduca sexta* has a packing ratio of 1:3 thick to thin filaments, the intensity of the 1,0 peak contains thick and thin filament mass, while the 2,0 peak is the sum of the second order harmonic of the 1,0 and the intensity due to layers containing only thin filaments (Fig: 1). As cross bridges move towards the thin filaments, there is a decrease of the 1,0 intensity due to the shifting of mass towards the layers of thin filaments. In contrast, the 2,0 stays relatively constant since there is little change in the total mass on these planes. Therefore the ratio of 2,0 to 1,0 intensity is expected to be highest during peak cross bridge binding. This differs from vertebrate muscle, where the ratio of the 1,1 reflection and 1,0 reflection is a surrogate for cross bridge binding. The intensities of the 1,0 and 2,0 reflections were computed using Musclex's "Equator" function, which first sets a box around the equator, uses convex hull background subtraction, and finally calculates peak intensity.

Lattice spacing

Lattice spacing was measured by tracking the 1,0 reflection's centroid motion using Musclex's Equatorial function and a Voigt model fitted to three peaks: 1,0; 1,1 and 2,0. This data was gathered simultaneously with cross bridge recruitment. Notably, the Voigt model we used within the Equator function's framework is overdetermined with only two peaks, so we tracked the 1,1 reflection intensity in the fit model as well. The distance of the centroid of the 1,0 equatorial reflection from the backstop correlates by Bragg's law to the distance between layers of the filament lattice containing the thick filament.

Filament strain

Thick and thin filament strain were calculated using axial filament spacing changes recorded along the meridian and in layer lines of the diffraction pattern. We used Musclex's Diffraction Centroids function to estimate the axial spacing of the following intensity peaks: the 14.4 nm meridional, an indicator of spacing changes between layers of myosin crowns; the 7.3 nm meridional, an indicator of spacing changes in the myosin containing thick filament backbone; and the 5.9 and 5.1 nm off meridional actin layer lines, which correspond to the pitches of the left and right genetic helices. At the exposure times we used, the actin layer lines were relatively weak. The 5.9 nm layer line intermittently yielded reliable data, while the 5.1 nm layer line was not measurable for most trials. The data presented for the 5.9 nm layer line should be interpreted with due caution since without 5.1 nm data filament twisting and stretching cannot be differentiated.

Data Handling

All of the code we used can be found in the GitHub repository: In_vivo_Myofilament_Lattice_Kinematics.

Permutation bootstrap

To assess if a signal contained significant cyclic changes at the same frequency as the muscle's activation we used a permutation bootstrap. We took the Fourier transform of a time series signal, which returned the power of the signal across frequency space. We then compared the power of the raw signal at wing beat frequency to the power obtained for a signal composed of the original signal, but randomly shuffled. If out of 1,000 permutations, fewer than 5% had a power greater than or equal to the original signal's power at wing beat frequency the signal was used to compute average periodic excursions. If more than 5% had a power greater than or equal to the original signal's, we cannot evaluate what component of the data is noise, so the signal was excluded from computing excursions. Out of the 11 trials we recorded, 10 showed significant periodic changes in lattice spacing, 9 showed significant periodic changes in cross bridge recruitment, 7 showed significant periodic thick filament stretch and 6 showed significant periodic thin filament stretch. These results correspond to the annotator's observations that data encoded on the equator is typically much stronger, while at the exposures lengths we used data encoded along the meridian was more challenging to track.

Spike Triggered Average (STA)

The STA is created by phase averaging time course x-ray diffraction data using the muscle's depolarization as the start point. One phase is defined to be the period of time between sequential membrane depolarizations (the interspike interval). Interspike intervals were denoted using Python scripts which identify EMG peaks and down sample their time resolution to that of the x-ray data, indicating the frame during which depolarization occurred.

Correlation

The correlation of signals as a function of proportion of interspike interval lag was used to determine if there was a consistent phase offset of cross bridge recruitment and thick filament stretch, and of cross bridge recruitment and lattice spacing change across trials. We also calculated the correlation of two signals as a function of absolute time lag (Fig: S3) and found no consistent pattern. Correlation was calculated using Numpy's built in correlation function.

Gradient boosted decision tree mechanism-free model (xGBoost)

xGBoost is a library to create gradient boosted decision trees that can be used for regression, classification and prediction (39). Gradient boosting iteratively combines weak hypotheses (in the case of xGBoost a weak hypothesis is a decision tree that has an imperfect prediction) that follow the gradient descent of an error loss function. At each iteration, a new tree is added with the goal of fixing the error left in the model prediction from the previous iterations. The loss function can be generalized as any differentiable function. xGBoost is a particularly fast and effective implementation of the machine learning algorithm 'gradient boosted decision trees' that has been used to win many Kaggle competitions (43). We used it to create a mechanism free prediction of lattice dilation from filament stretching and cross bridge recruitment data. Specifically, the model was trained using data from the 14.4 nm reflection's intensity (often used as an indicator of cross bridge recruitment in vertebrate systems), the ratio of the reflections of the 2,0 and 1,0 planes, the 7.3 nm reflection's centroid and the 5.9 nm off meridional's centroid. Since the change of the lattice's shape from one timestep to the next depends not only on the state of these parameters, but also their time history, we extended the information available to the model by including the time history of cross bridge recruitment and filament stretching up to 0.03 seconds prior to the time point to be predicted. In the interest of reproducibility, the model's hyperparameters can be found in the supplement (Supplement: xGBoost).

Acknowledgements

The authors gratefully acknowledge the thoughtful feedback of Joseph Powers, Abigail von Hagel and Michael Regnier on muscle biophysics; and the feedback of Callin Switzer, Satpreet Singh and Bingni Brunton on data analysis.

Competing interests

The authors declare no competing interests

Funding

This research used resources of the Advanced Photon Source, a U.S. Department of Energy (DOE) Office of Science User Facility operated for the DOE Office of Science by Argonne National Laboratory under Contract No. DE-AC02-06CH11357. Use of the Pilatus 3 1M detector was provided by grant 1S10OD018090-01 from the NIH. This project was supported by grant 9 P41 GM103622 from the National Institutes of Health; grant W911NF-14-1-0396 from the Army Research Office to TLD and the Joan and Richard Komen Endowed Chair to TLD. SAM was supported by the Bioengineering Cardiac Training Grant (NIH/NIBIB T32EB1650) and a fellowship from the ARCS foundation. AMA was supported by NIH P30AR074990. The content is solely the responsibility of the authors and does not necessarily reflect the official views of the National Institutes of Health.

REFERENCES

[1]Michael H. Dickinson, Claire T. Farley, Robert J. Full, M. A. R. Koehl, Rodger Kram, and Steven Lehman. How animals move: An integrative view. Science, 288(5463):100–106, 2000.

[2]C. David Williams, Mary K. Salcedo, Thomas C. Irving, Michael Regnier, and Thomas L. Daniel. The length–tension curve in muscle depends on lattice spacing. Proceedings of the Royal Society of London B: Biological Sciences, 280(1766), 2013.

[3]NT George, TC Irving, CD Williams, and TL Daniel. The cross-bridge spring: can cool muscles store elastic energy? Science, 340(6137):1217–1220, 2013.

[4]NT George, S Sponberg, and TL Daniel. Temperature gradients drive mechanical energy gradients in the flight muscle of manduca sexta. Journal of Experimental Biology, 215(3):471–479, 2012.

[5]K. Wakabayashi, Y. Sugimoto, H. Tanaka, Y. Ueno, Y. Takezawa, and Y. Amemiya. X-ray diffraction evidence for the extensibility of actin and myosin filaments during muscle contraction. Biophysical Journal, 67(6):2422 – 2435, 1994.

[6]Thomas L Daniel, Alan C Trimble, and P Bryant Chase. Compliant realignment of binding sites in muscle: transient behavior and mechanical tuning. Biophysical Journal, 74(4):1611–1621, 1998.

[7]John M Squire. Architecture and function in the muscle sarcomere. Current opinion in structural biology, 7(2):247–257, 1997.

[8]Michael Dickinson, Gerrie Farman, Mark Frye, Tanya Bekyarova, David Gore, David Maughan, and Thomas Irving. Molecular dynamics of cyclically contracting insect flight muscle in vivo. Nature, 433(7023):330, 2005.

[9]TC Irving and DW Maughan. In vivo x-ray diffraction of indirect flight muscle from drosophila melanogaster. Biophysical journal, 78(5):2511–2515, 2000.

[10]H Iwamoto and N Yagi. The molecular trigger for high-speed wing beats in a bee. Science, 341(6151):1243–1246, 2013.

[11]Douglas A Syme and Robert K Josephson. How to build fast muscles: synchronous and asynchronous designs. Integrative and comparative biology, 42(4):762–770, 2002.

[12]Michael S. Tu and Thomas L. Daniel. Cardiac-like behavior of an insect flight muscle. Journal of Experimental Biology, 207(14):2455–2464, 2004.

[13]Alex Gomez-Marin and Asif A Ghazanfar. The life of behavior. Neuron, 104(1):25–36, 2019.

[14]Massimo Reconditi, Elisabetta Brunello, Marco Linari, Pasquale Bianco, Theyencheri Narayanan, Pierre Panine, Gabriella Piazzesi, Vincenzo Lombardi, and Malcolm Irving. Motion of myosin head domains during activation and force development in skeletal muscle. Proceedings of the National Academy of Sciences, 108(17):7236–7240, 2011.

[15]AM Gordon, E Homsher, and M Regnier. Regulation of contraction in striated muscle. Physiological reviews, 80(2):853–924, 2000.

[16]John M Squire and Edward P Morris. A new look at thin filament regulation in vertebrate skeletal muscle. The FASEB Journal, 12(10):761–771, 1998.

[17]Julian E Stelzer, Daniel P Fitzsimons, and Richard L Moss. Ablation of myosin-binding protein-c accelerates force development in mouse myocardium. Biophysical journal, 90(11):4119–4127, 2006.

[18]BERND HEINRICH and GEORGE A BARTHOLOMEW. An analysis of pre-flight warm-up in the sphinx moth, manduca sexta. Journal of Experimental Biology, 55(1):223–239, 1971.

[19]Thomas C Irving. X-ray diffraction of indirect flight muscle from drosophila in vivo. In Nature's Versatile Engine: Insect Flight Muscle Inside and Out, pages 197–213. Springer, 2006.

[20]Sergey Y Bershitsky, Michael A Ferenczi, Natalia A Koubassova, and Andrey K Tsaturyan. Insight into the actin-myosin motor from x-ray diffraction on muscle. Frontiers in Bioscience, 14(8):3188–3213, 2009.

[21]Jeffrey J Harford and JohnM Squire. Evidence for structurally different attached states of myosin cross-bridges on actin during contraction of fish muscle. Biophysical journal, 63(2):387–396, 1992.

[22]Zhongjun Hu, Dianne W Taylor, Michael K Reedy, Robert J Edwards, and Kenneth A Taylor. Structure of myosin filaments from relaxed lethocerus flight muscle by cryo-em at 6 å resolution. Science advances, 2(9):e1600058, 2016.

[23]MK Reedy, JM Squire, BAJ Baumann, A Stewart, and TC Irving. X-ray fibre diffraction of the indirect flight muscle of lethocerus indicus. Advanced Photon Source User Activity: Report, 2000.

[24]E Brunello, P Bianco, G Piazzesi, M Linari, M Reconditi, P Panine, T Narayanan, WI Helsby, M Irving, and V Lombardi. Structural changes in the myosin filament and cross-bridges during active force development in single intact frog muscle fibres: stiffness and x-ray diffraction measurements. The Journal of physiology, 577(3):971–984, 2006.

[25]Hugh E Huxley, Alex Stewart, Hernando Sosa, and Tom Irving. X-ray diffraction measurements of the extensibility of actin and myosin filaments in contracting muscle. Biophysical journal, 67(6):2411–2421, 1994.

[26]Richard L Moss and Daniel P Fitzsimons. Frank-starling relationship: long on importance, short on mechanism, 2002.

[27]M Schoenberg. Geometrical factors influencing muscle force development. ii. radial forces. Biophysical journal, 30(1):69–77, 1980.

[28]C David Williams, Michael Regnier, and Thomas L Daniel. Elastic energy storage and radial forces in the myofilament lattice depend on sarcomere length. PLoS computational biology, 8(11):e1002770, 2012.

[29]C. David Williams, Michael Regnier, and Thomas L. Daniel. Axial and radial forces of cross-bridges depend on lattice spacing. PLOS Computational Biology, 6(12):1–10, 12 2010.

[30]David A Smith. Electrostatic forces or structural scaffolding: What stabilizes the lattice spacing of relaxed skinned muscle fibers? Journal of theoretical biology, 355:53–60, 2014.

[31]Barry M. Millman. The filament lattice of striated muscle. Physiological Reviews, 78(2):359–391, 1998. PMID: 9562033.

[32]M.A. Bagni, G. Cecchi, P.J. Griffiths, Y. Maéda, G. Rapp, and C.C. Ashley. Lattice spacing changes accompanying isometric tension development in intact single muscle fibers. Biophysical Journal, 67(5):1965 – 1975, 1994.

[33]Weikang Ma, Henry Gong, Balázs Kiss, Eun-Jeong Lee, Henk Granzier, and Thomas Irving. Thick-filament extensibility in intact skeletal muscle. Biophysical Journal, 115(8):1580 – 1588, 2018.

[34]Chen-Ching Yuan, Weikang Ma, Peter Schemmel, Yu-Shu Cheng, Jiangmin Liu, George Tsaprailis, Samuel Feldman, Agnes Ayme Southgate, and Thomas C Irving. Elastic proteins in the flight muscle of manduca sexta. Archives of biochemistry and biophysics, 568:16–27, 2015.

[35]Joseph D Powers, C David Williams, Michael Regnier, and Thomas L Daniel. A Spatially Explicit Model Shows How Titin Stiffness Modulates Muscle Mechanics and Energetics. Integrative and Comparative Biology, 58(2):186–193, 06 2018.

[36]John Trinick. Cytoskeleton: titin as a scaffold and spring. Current Biology, 6(3):258–260, 1996.

[37]L Tskhovrebova, J Trinick, JA Sleep, and RM Simmons. Elasticity and unfolding of single molecules of the giant muscle protein titin. Nature, 387(6630):308, 1997.

[38]Belinda Bullard, Tzintzuni Garcia, Vladimir Benes, Mark C Leake, Wolfgang A Linke, and Andres F Oberhauser. The molecular elasticity of the insect flight muscle proteins projectin and kettin. Proceedings of the National Academy of Sciences, 103(12):4451–4456, 2006.

[39]Tianqi Chen and Carlos Guestrin. Xgboost: A scalable tree boosting system. In Proceedings of the 22nd acm sigkdd international conference on knowledge discovery and data mining, pages 785–794. ACM, 2016.

[40]John L Eaton et al. Lepidopteran anatomy. John Wiley & Sons Limited, 1988.

[41]R Fischetti, S Stepanov, G Rosenbaum, R Barrea, E Black, D Gore, R Heurich, E Kondrashkina, AJ Kropf, S Wang, et al. The biocat undulator beamline 18id: a facility for biological non-crystalline diffraction and x-ray absorption spectroscopy at the advanced photon source. Journal of synchrotron radiation, 11(5):399–405, 2004.

[42]J Jiratrakanvong, J Shao, M Menendez, X Li, J Li, W Ma, G Agam, and T Irving. Musclex: software suite for diffraction x-ray imaging v1. 13.1, 2018.

[43]Alexis Cook. Intermediate machine learning.